pharmaceuticals

MDPI

Article

Unexpected salt/co-crystal polymorphism of the ketoprofen-lysine system: discovery of a new ketoprofen-L-lysine salt isoform with different physicochemical and pharmacokinetic properties

Andrea Aramini [1,*], Gianluca Bianchini [1], Samuele Lillini [2,3], Simone Bordignon[4], Mara Tomassetti [2], Rubina Novelli [5], Simone Mattioli [2], Larisa Lvova [6], Roberto Paolesse [6], Michele Remo Chierotti [4] and Marcello Allegretti [1]

[1] Research and Early Development, Dompé Farmaceutici S.p.A., L'Aquila, Italy;
[2] Research and Early Development, Dompé Farmaceutici S.p.A., Napoli, Italy;
[3] IMAST S.c.a.r.l. - Technological District on Engineering of polymeric and composite Materials and Structures, Napoli, Italy
[4] Department of Chemistry and NIS Centre, University of Torino, Torino, Italy;
[5] Research and Early Development, Dompé Farmaceutici S.p.A., Milano, Italy;
[6] Department of Chemical Science and Technology, University of Rome Tor Vergata, Rome, Italy;

* Correspondence: andrea.aramini@dompe.com;

Abstract: Ketoprofen-L-lysine salt (KLS) is a widely used non-steroidal anti-inflammatory drug. Here, we studied deeply the solid-state characteristics of KLS to possibly identify new polymorphic drugs. Conducting a polymorph screening study and combining conventional techniques with solid-state nuclear magnetic resonance, we identified, for the first time, a salt/co-crystal polymorphism of the ketoprofen (KET)-lysine (LYS) system, with the co-crystal, KET-LYS polymorph 1 (P1), being representative of commercial KLS, and the salt, KET-LYS polymorph 2 (P2), being a new polymorphic form of KLS. Interestingly, in vivo pharmacokinetics showed that the salt isoform has significantly higher absorption and thus a different pharmacokinetics compared to commercial KLS (co-crystal), laying the basis for the development of faster release/acting KLS formulations. Moreover, intrinsic dissolution rate (IDR) and electronic tongue analyses showed that the salt has a higher IDR, a more bitter taste and a different sensorial kinetics compared to the co-crystal, suggesting that different coating/flavouring processes should be envisioned for the new compound. Thus, the new KLS polymorphic form with its different physicochemical and pharmacokinetic characteristics can open the way to the development of a new KET-LYS polymorph drug that can emphasize the properties of commercial KLS for the treatment of acute inflammatory and painful conditions.

Keywords: Ketoprofen-L-lysine salt; co-crystal; salt; polymorphism; faster release formulation.

Citation: Lastname, F.; Lastname, F.; Lastname, F. Title. *Pharmaceuticals* **2021**, *14*, x. https://doi.org/10.3390/xxxxx

Academic Editor: Firstname Lastname

Received: date
Accepted: date
Published: date

1. Introduction

During the last decade, co-crystallization has emerged and established itself in the field of pharmaceutical solid-state chemistry as an advanced and valuable method to modify the physicochemical characteristics of drugs[1]. Like pharmaceutical salts, co-crystals are multi-component crystalline solid materials formed by two or more molecules, of which at least one is an active pharmaceutical ingredient (API) that is combined with safe, organic molecules used as co-crystallizing agents, or coformers[2]. Pharmaceutical salts and co-crystals thus preserve the intrinsic activities of the APIs, while their physicochemical properties can be tailored systematically by varying the coformers[3]. Contrary to salts however, in which the molecules within the crystal lattice predominantly interact through ion pairing[4], in co-crystals the components are combined via non-covalent interactions (e.g. hydrogen bonds, van der Waals forces, π-stacking, and electrostatic interactions) in a definite stoichiometric ratio[5,6]. Thus, co-crystals can be distinguished from salts because in these latter ones a complete proton transfer occurs along the axis of the hydrogen bond (HB) interaction between the API and the molecular partner, while in co-crystals a neutral adduct is formed by the components[7].

Most commonly, when a specific pair of molecules is combined with the same stoichiometry and at the same temperature, the outcome is either a salt (ionic) or a co-crystal (neutral)[8]. However, to predict whether the outcome will be one or the other can be difficult. For this reason, a "p*Ka* rule" has been proposed to provide, at least to some extent, reliable indications about the possibility to obtain a salt and vice versa. Accordingly, the larger the Δp*Ka* [i.e. p*Ka*(protonated base) - p*Ka*(acid)], the greater the chance to obtain a salt and vice versa [9–11], and the probability can also be quantitatively estimated with formulas (Pobs(AB)/% = -17Δp*Ka* + 72 and Pobs(A-B+)/% = 17Δp*Ka* + 28 for the salt and the co-crystal, respectively)[10]. These formulas identify a region of uncertainty around Δp*Ka* = 1, wherein the chances to get a salt or a co-crystal are very similar. In this region usually fall the rare cases in which the same chemical species can give rise to both a co-crystal and a salt (salt/co-crystal polymorphism), which have the same composition and stoichiometry at the same temperature, depending on the crystallization protocol. Stainton et al. were the first reporting a co-crystal and a salt of the same chemical composition – isonicotinamide and citric acid – [12], and subsequently, other salt/co-crystal polymorphisms were obtained from β-alanine and DL-tartaric acid[13,14], sulfamethazine and saccharine[15], dinitrobenzoic acid and haloanilines[16], and ethionamide and salicylic acid[8]. Some of these systems have been analysed for their thermodynamic stability[14], moisture sorption and compaction properties[15], or dissolution rate[8], and co-crystals resulted to have superior or similar properties compared to those of the polymorphic salts. Only a limited number of these studies, however, compare head-to-head salt and co-crystal polymorphic forms originated from the same chemical species in terms of physicochemical properties and *in vivo* pharmacokinetic and pharmacodynamic properties, leaving still open the question about the actual impact that the physicochemical difference between salt and co-crystal polymorphic forms can have on the clinical performance/pharmacological properties of a drug. Answering this question is of particular interest, not only because of the regulatory and legal implications of intellectual property rights related to the discovery of a new isoform[17], but most importantly because it could lead to the development of a drug that, while maintaining the same chemical composition of the polymorphic one, can have different pharmacokinetic and pharmacological characteristics. Based on its physicochemical and pharmacokinetic properties, the polymorphic form may allow for the development of different formulations[18], which can be characterized, for example, by a slower or faster drug release in the blood; on the other hand, based on its taste, a different coating process or flavour can be used to mask the drug taste, thus possibly affecting drug manufacturing costs and patient compliance[19]. Finally, based on all the pharmacokinetic and physicochemical characteristics of the new isoform, also new therapeutic indications can potentially be hypothesized.

With the aim of studying deeply the solid-state characteristics of ketoprofen-L-lysine salt (KLS) to identify all its crystalline forms and thus possibly discover new polymorphic drugs, we thoroughly investigated, for the first time, the existence of polymorphic isoforms of the ketoprofen (KET)-lysine (LYS) system (Scheme 1). KET belongs to the non-steroidal anti-inflammatory drugs (NSAIDs), widely used anti-inflammatory, analgesic and antipyretic compounds that are usually marketed in different forms with sodium, lysine, arginine, and others, to improve the physicochemical and pharmacological profile of the APIs[20,21]. Indeed, KET-salts like KLS have significantly higher solubility compared to KET, allowing for a more rapid absorption of the drug and a subsequent faster onset of the therapeutic effects after oral administration[22].

Here, we report the synthesis and characterization of two distinct KET-LYS polymorphic forms, respectively with salt and co-crystal structural characteristics, and compared their physicochemical properties, organoleptic characteristics by electronic tongue analysis and their pharmacokinetics *in vivo*.

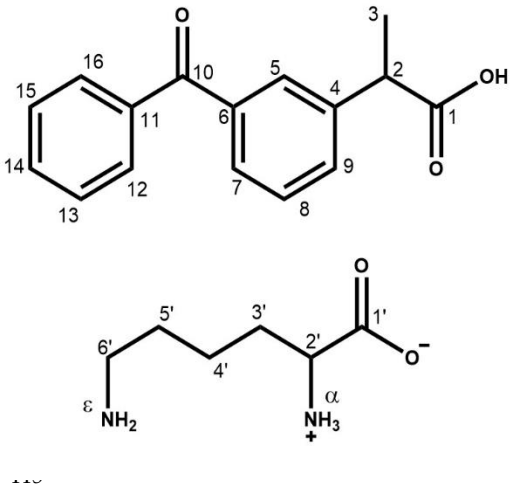

Scheme 1. Molecular representation of KET (top) and LYS (bottom), with C and N atom labelling.

2. Results and Discussion

2.1. Crystallization conditions and identification of KET-LYS polymorphs

As part of a project aimed at the identification of new polymorphs of the KET-LYS system, we obtained two polymorphic forms of KET-LYS, KET-LYS P1 and KET-LYS P2, through different crystallization techniques. We performed more than 230 experiments and analysed all the collected solids by X-ray Powder Diffractometry (XRPD) analysis and compared them with the starting material. Mechanochemistry methods were ineffective, as grinding and kneading experiments led to the isolation of solids having the same diffraction pattern of the starting material although presenting a lower crystallinity degree. Evaporation and slurry experiments in different conditions led to only unstable and amorphous phases. The best results were obtained performing several precipitation experiments by anti-solvent addition as described in Materials and Methods. We analysed the solids obtained using this latter method and deeply characterized them using advanced crystalline solid-state technologies

2.2. Characterization of synthesized KET-LYS P1 and P2

According to the p*Ka* rule, the reaction between KET and LYS should result in a salt, as the Δp*Ka* of these molecules is 5.84 (p*Ka*(protonated LYS γ-NH2) - p*Ka*(KET COOH) = 10.29 - 4.45). However, since the model suggested by Cruz-Cabeza et al.[10] is validated only for -1 < Δp*Ka* < 4 and Δp*Ka* in this case is higher than 4, the probabilities of obtaining a salt or a co-crystal cannot be quantitatively estimated.

Since crystals of suitable size for single crystal X-ray diffraction could not be produced, we performed an XRPD analysis to investigate the microstructure and properties of the powders. The non-superimposition of the XRPD diffraction patterns (Figure 1) showed the presence of two different phases with different crystalline degree that were called KET-LYS Polymorph 1 (P1) and KET-LYS Polymorph 2 (P2).

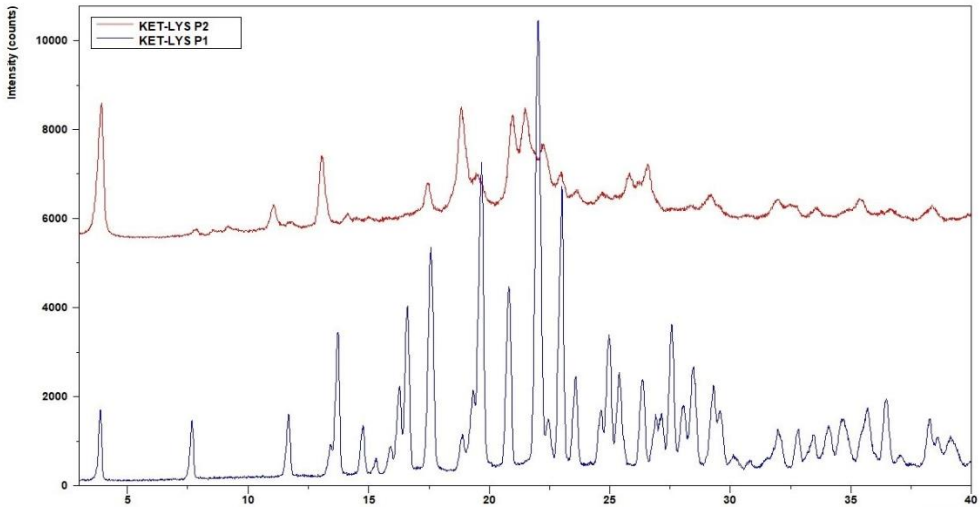

Figure 1. Comparison between XRPD patterns of KET-LYS P1 and KET-LYS P2. The diffraction patterns of KET-LYS P1 and KET-LYS P2 are non-superimposable.

To define the nature of these two polymorphs, we firstly performed a differential scanning calorimetry (DSC). Interestingly, the DSC profile of KET-LYS P1 showed an endothermic event at 170.7 °C (onset 164.1 °C) that was associated with sample melting and degradation (Figure S1), while, on the other hand, the DSC profile of KET-LYS P2 showed multiple endothermic peaks, the first one at 110.9 °C (onset 100.5 °C), while above 120 °C, multiple partially overlapped endothermic peaks were detectable due to degradation steps (Figure S2).

We then performed an FT-IR analysis and observed that the vibration peaks of the KET-LYS system characteristic functional groups (O-H, N-H, and COOH) significantly differed between the two polymorphs, and this could be attributable to hydrogen bonding and salt formation (Figure S3 and S4). Indeed, in KET-LYS P1, the IR band was centered around 3160 cm^{-1} and could represent the OH stretching in carboxylic acid dimer bands; on the contrary, this band was not detectable in KET-LYS P2, which showed instead a very broad band at 3400 - 3660 cm^{-1}. Finally, in KET-LYS P2, the strong band at 1.550 cm^{-1} could be due to KET carboxylate anion group[26].

Starting from these preliminary evidences, we then performed a solid-state nuclear magnetic resonance (SSNMR), relying on the accuracy of this technique[27] to undoubtedly determine the ionic or neutral nature of our samples. Both ^{13}C and ^{15}N chemical shifts are in fact very sensitive to the protonation state of carboxylic and N-containing functional

groups[28]. In general, the carboxylic ^{13}C chemical shift undergoes a high-frequency shift in this order: neutral carboxylic groups (COOH) < COOH involved in HB interactions (COOH···X) < formation of a dimer through a homosynthon (COOH···HOOC) ≈ carboxylate groups (COO-)[27]; the 15N chemical shift is even more sensitive, as protonation induces shifts that can be as large as 25 ppm towards higher frequencies for aliphatic amines in agreement with the minor contribution of the lone pair to ⊚ploc[27]. 1D (^{13}C and ^{15}N CPMAS) and 2D (^{1}H-^{13}C HETCOR) experiments were acquired for KET-LYS P1 and the ^{13}C CPMAS spectrum was acquired for KET-LYS P2. For comparison, we also analysed pure KET, its sodium salt (Na^+KET^-), DL-LYS·2HCl and pure L-LYS, the latter being selected as reference due to its crystal structure displaying a free ε-NH2 group (Figure S5). Table 1 lists ^{13}C and ^{15}N chemical shifts of KET-LYS P1 and KET-LYS P2 with assignments.

Table 1. ^{13}C and ^{15}N SSNMR chemical shift assignments for KET-LYS P1 and KET-LYS P2. Please, refer to Scheme 1 for atom labeling.

KET-LYS P1		**KET-LYS P2**	
^{13}C			
^{13}C δ (ppm)	**C atom**	**^{13}C δ (ppm)**	**C atom**
196.1	10	194.5	10
177.6	1	181.5	1
174.5	1'	176.1	1'
147.4	6	145.1	6
141.0	11	139.7	11
134.8	4	138.1	4
133.0	Aromatic CH	133.4	Aromatic CH
128.8	Aromatic CH	131.8	Aromatic CH
128.3	Aromatic CH	129.8	Aromatic CH
128.0	Aromatic CH	128.8	Aromatic CH
126.8	Aromatic CH	127.7	Aromatic CH
55.1	2'	53.2	2'
50.2	2	47.4	2
38.8	6'	34.5	6'
32.2	5'	25.9	5'+3'
29.6	3'	21.2	3
24.7	3	16.6	4'
22.3	4'	/	/
^{15}N			
^{15}N δ (ppm)	**N atom**		
43.0	α		
32.8	ε		

The ^{13}C CPMAS spectra of KET-LYS P1 and KET-LYS P2 exhibited consistent shifts in the resonances associated both with KET and L-LYS carbon atoms (Figure S6). These data are in line with the formation of two novel crystal forms that differ from each other and from the starting materials. The samples are pure, as no residual peaks of the starting materials are present, and both crystal forms contain one independent molecule of KET and one of LYS. The fact that the starting materials are racemic suggests the presence of an inversion center in both crystal forms. Moreover, the average full width at half maximum (FWHM) value for the signals indicates a high and a low degree of crystallinity for KET-LYS P1 (~65 Hz) and KET-LYS P2 (~130 Hz), respectively.

In Figure 2, the C=O regions (170-210 ppm) of the ^{13}C CPMAS spectra of KET, (L)-LYS, Na^+KET^-, KET-LYS P1 and KET-LYS P2 are reported. Analyzing the ^{13}C CPMAS spectrum of KET, a signal is detectable at 184.0 ppm, a high value that is typical, and thus indicative, of a carboxylic group involved in a homodimeric interaction (as is the case for KET, Figure S7)[29]; on the other hand, its sodium salt Na^+KET^- displays two peaks at 181.4 and 180.5 ppm, which indicate the presence of two independent molecules in the unit cell. Both these chemical shifts are consistent with the unprotonated nature of a carboxylate group (COO-). In the case of KET-LYS P1, we observed two peaks in the carboxylic region, at 174.5 and 177.6 ppm.

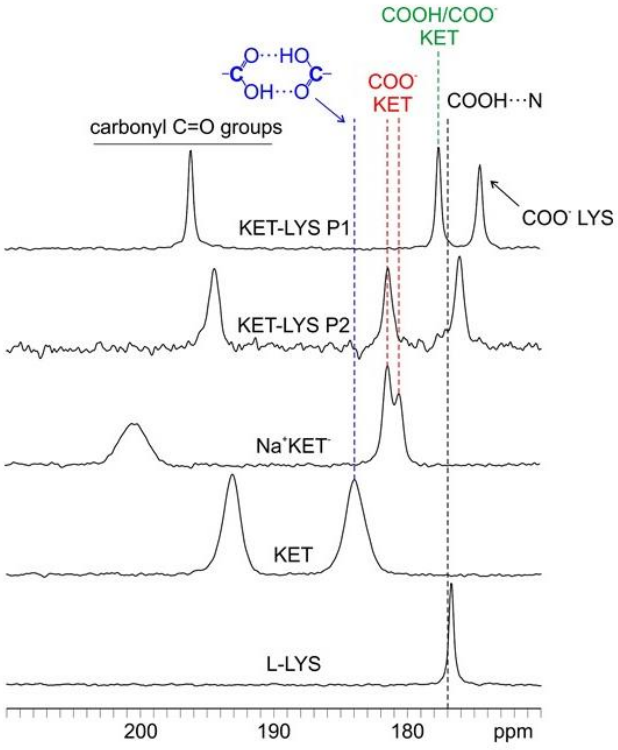

Figure 2. Carboxylic region (170-210 ppm) of the ^{13}C CPMAS spectra of samples KET, L-LYS, Na^+KET^-, KET-LYS P1 and KET-LYS P2. The black dashed line at ca. 177 ppm refers to the chemical shift reported in literature for the protonated carboxylic group of ibuprofen, involved in a HB interaction with a nitrogen atom, in a (ibuprofen)2(4,4'-bipyridyl) co-crystal[30].

To understand which signal refers to the carboxylic group of KET and which to the one of LYS, we performed a 2D experiment (namely, ^1H-^{13}C FSLG HETCOR) in two different versions, with on- and off-resonance CP conditions: the first (Figure S8) allowed observing

short-range correlations only between covalently bonded C atoms and protons; the second one (Figure 3) provided signals also for long-range interactions between C and H nuclei which are spatially close, within 3-4 Å. The short-range experiment (Figure S8) made it possible to correlate the 13C signals of the CH groups of LYS (55.1 ppm) and KET (50.2 ppm) to the corresponding protonic peaks, leading to their assignment at 3.4 and 3.6 ppm, respectively. Being the CH groups the closest to the carboxylic moieties in both KET and LYS, we were then able, through the long-range version of the experiment (Figure 3), to identify the carboxylic signal of LYS at 174.5 ppm (correlating with the protonic signal at 3.4 ppm) and that of KET at 177.6 ppm (correlating with the protonic signal at 3.6 ppm). The carboxylic peak of LYS agrees with the typical chemical shift of the COO- in pure LYS (176.7 ppm), which, together with the ^{15}N data (see below), confirms the zwitterionic nature of LYS in KET-LYS P1. The KET signal resonates at a frequency which is much lower than that of both the COO- groups of $Na^{+}KET^{-}$ (181.4/180.5 ppm) and the homodimeric COOH group of pure KET (184.0 ppm). In particular, the KET signal is very similar to that unambiguously assigned to a neutral carboxylic group involved in a HB, observed at ca. 177 ppm in the (ibuprofen)2(4,4'-bipyridyl) co-crystal[30]. Since the carboxylic environment of ibuprofen is very similar to that of KET, the comparison we made is definitely reliable. Thus, these data suggest that the carboxylic group of KET in KET-LYS P1 is in a protonated state (COOH) and involved in HBs with LYS, making KET-LYS P1 better defined as a co-crystal rather than a salt.

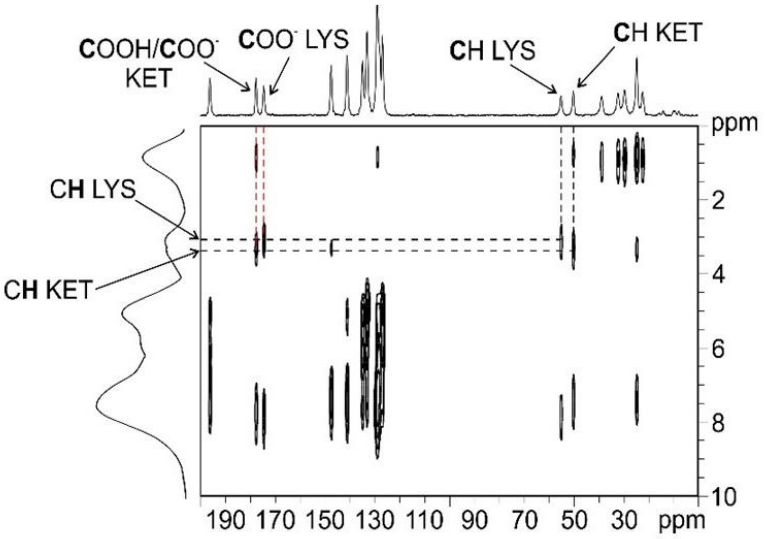

Figure 3. Off-resonance ^{1}H-^{13}C FSLG HETCOR spectrum (contact time = 7 ms) of KET-LYS P1. Above, ^{13}C spectrum; on the left, ^{1}H spectrum. Black dashed lines represent significant correlations among covalently bonded protons and C atoms in the crystal structure; red dashed lines represent significant correlations among protons and C atoms spatially close in the crystal structure (see main text). Spinning speed of 12 kHz, room temperature.

To confirm this assumption, we further investigated the system by ^{15}N CPMAS SSNMR analysis, which usually offers the chance to discriminate between deprotonated and protonated N atoms, and thus in this case between the NH_2 and NH_3^{+} moieties of (L)-LYS and KET-LYS P1. Figure 4 shows the ^{15}N CPMAS NMR spectra of samples (L)-LYS, (DL)-LYS·2HCl and KET-LYS P1. (L)-LYS itself contains both types of moieties: its ε-NH2 group, free from HBs (as observable in its crystal structure, Figure S5 and ref[31]), resonates at 27.2 ppm, while its α-NH_3^{+} falls at 41.0 ppm. The ^{15}N CPMAS spectrum of KET-LYS P1 allowed confirming the protonated nature of the α-NH_3^{+} of LYS in KET-LYS P1

(43.0 ppm), and showed that the ε-N signal falls at 32.8 ppm, which is intermediate between the chemical shifts of α-NH_3^+ and ε-NH_2 of pure (L)-LYS. Although ambiguous, its chemical shift suggests the presence of a neutral NH_2 group involved in HB interactions, i.e. $H_2N\cdots H$-X. Indeed, a proper ε-NH_3^+ signal falls at 41.3 ppm as observed in the spectrum of (DL)-LYS·2HCl. Thus, it can be said that this system falls in the salt/co-crystal continuum but pointing more towards a neutral nature and again supporting the concept that KET-LYS P1 structure is more referable to a co-crystal rather than to a salt.

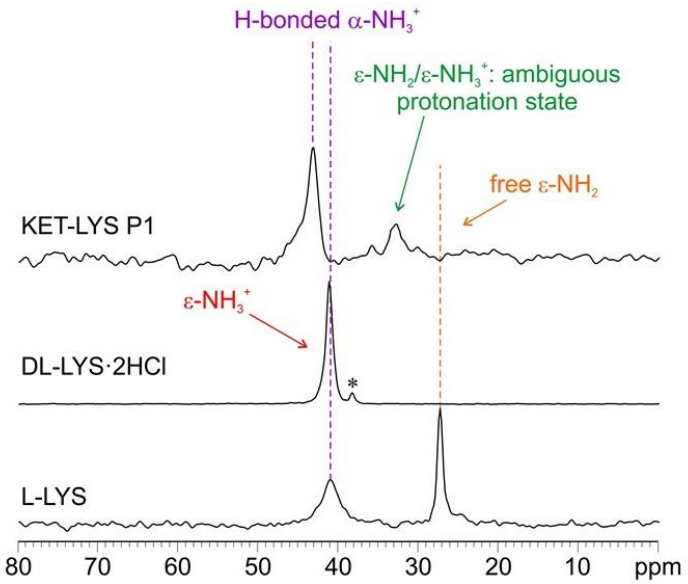

Figure 4. ^{15}N (40.6 MHz) CPMAS spectra of samples L-LYS, DL-LYS·2HCl and KET-LYS P1. Acquisition at room temperature at a spinning speed of 9 kHz. The asterisk in the middle spectrum identifies a small signal due to an impurity.

From the comparison among the ^{13}C CPMAS spectra, it can be observed how in KET-LYS P2 the signal at 181.5 ppm (referred to KET) is quite close to the signal of pure KET (184.0 ppm) and especially of Na^+KET^- (181.4/180.5 ppm). This suggests that in KET-LYS P2, the COOH of KET is in a carboxylate form, since dimeric COOH groups and COO- moieties resonate at similar frequencies.

All together these data clearly demonstrate that the crystallization outcome of the reaction between KET and LYS is a case of salt/co-crystal polymorphism. This result is unexpected if we consider the p*Ka* rule and the fact that the Δp*Ka* of our system is > 4, for which a salt is to be definitely expected. Thus, while the p*Ka* rule has a statistic and predictive value that is fundamental in the design phase, once the adduct is obtained, the characterization of the protonation state must be always supported by diffraction and/or spectroscopic data. This is because, as also for this system, the influence of crystalline environment in defining the hydrogen position along an HB is more important than the strength of the acidic and basic sites[11].

Surprisingly, the subsequent analysis of commercial samples of KLS from different manufacturers showed that it is representative of KET-LYS P1 (Figure S9), thus revealing that commercial KLS should be more appropriately defined as a co-crystal rather than a salt. The existence of a stable co-crystal structure of KET-LYS was not predictable based on the typical "p*Ka* rule", which has been validated only for a limited Δp*Ka* range[10]. Thus,

these new findings highlight the importance of conducting specific studies to assess the salt/co-crystal polymorphism possibility for species with a ΔpKa outside the $-1 < \Delta pKa < 4$ range.

2.3. Intrinsic dissolution rates of co-crystal KET-LYS P1 and salt KET-LYS P2

Having identified two distinct polymorphs of the KET-LYS system, we then analyzed these two isoforms in regard of some of the intrinsic chemical and physical properties that have to be considered before the development of a pharmaceutical formulation. Among these properties, the dissolution rate of a drug is usually modified by co-crystallization processes[2]. Thus, we investigated whether the co-crystal form of KET-LYS system (KET-LYS P1) has different intrinsic dissolution rate (IDR) compared to its salt polymorph (KET-LYS P2). The results showed two different IDRs from the two compact forms, having constant surface area exposed to the GSF medium (Figure 5 and Table 2). In particular, IDR comparative profile (Table 2) between KET-LYS P1 and KET-LYS P2 shows that the release of KET from KET-LYS P2 is significantly faster than from KET-LYS P1 at pH 1.2 (SGF) and KET-LYS P2 seems to have a higher IDR than KET-LYS P1.

Table 2. IDR (slope) $mgcm^{-1}min^{-1}$ of co-crystal KET-LYS P1 and salt KET-LYS P2.

	IDR (slope) $mgcm^{-1}min^{-1}$	confidence interval (95%)	
Co-crystal KET-LYS P1	1.453	1.411	1.495
Salt KET-LYS P2	1.907	1.813	2.002

These results further confirm that the outcomes of KET and LYS crystallization are two different structural entities and demonstrate that the two forms are characterized by different IDRs. *In vitro* dissolution is an important factor in defining drug absorption, distribution, metabolism and excretion (ADME), and different IDRs among drugs can allow for the development of formulations with different release kinetic profiles[32]. Commercial KLS (representative of KET-LYS P1) has been reported to exhibit fast *in vivo* absorption and onset of action[22]; thus, the faster dissolution observed for KET-LYS P2 compared to KET-LYS P1 may suggest that the newly synthesized salt form (KET-LYS P2) could be characterized by a faster absorption compared to the commercialized KLS.

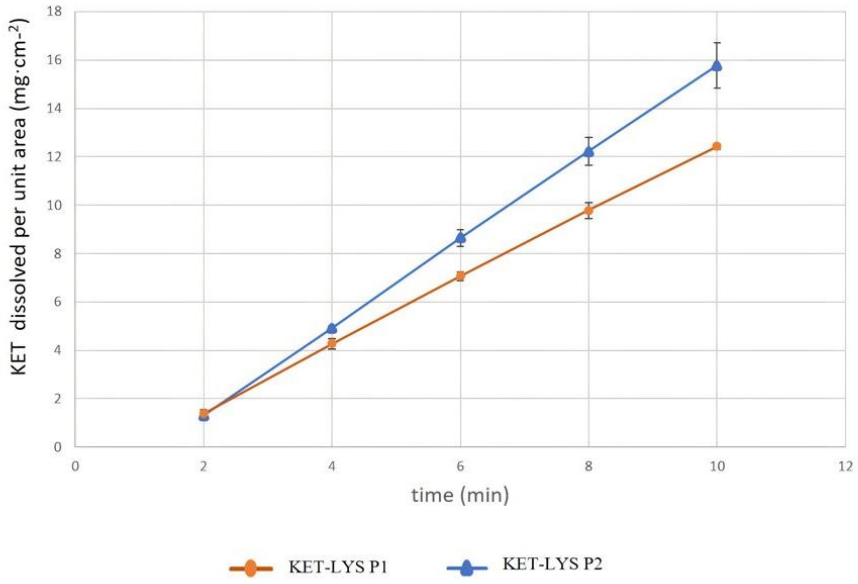

Figure 5. Intrinsic dissolution rates of co-crystal KET-LYS P1 and salt KET-LYS P2. Dissolution profiles of KET from KET-LYS P1 and KET-LYS P2, having constant surface area exposed to the dissolution medium. Three analytical replicates were performed for all the time points. Values are expressed as mean ± SD.

2.4. Taste and sensorial kinetic analysis of KET-LYS P1 and KET-LYS P2

One of the central challenges of drug manufacturing is to sweeten the unpleasant taste of APIs, which can be bitter, salty, sour, and even metallic or astringent, as it negatively affects the compliance of patients, especially in paediatric and geriatric populations[33]. Technologies have been developed to mask unpleasant drug tastes and odours, such as the use of physical barriers (coating), or the addition of sweeteners and flavouring excipients[34], but modifying the taste of a drug is not an easy, straightforward process, as it strongly depends on the target patient age and geographic location[35], and, of course, on the API itself[36]. Thus, drugs that, at the beginning of their development, have different tastes, will potentially allow for different subsequent coating processes or flavour addition.

As some studies have reported, the taste of a drug is among the chemical properties that co-crystallization can modify[2]. For example, co-crystals of hydrochlorothiazide obtained using sucralose as a coformer had increased dissolution rate and taste masking compared to the API[37], while taste sensing experiments revealed the sweetness of the co-crystal of paracetamol with trimethylglycine due to the presence of the latter one in the structure[38], and of the co-crystal obtained from theophylline and saccharine[39].

We thus investigated and compared the taste and the sensorial kinetics of KET-LYS P1 and KET-LYS P2, to assess whether the substitution of an ionic bond (salt) with a neutral HB (co-crystal) – rather than the substitution or the addition of coformers as described in the above examples – can alter these characteristics. To analyse the variation of bitterness and palatability characteristics of KET and LYS pharmaceutical preparations, we used a potentiometric E-tongue system application, a method that was successfully employed in previous researches dedicated to the evaluation of soft cheeses salinity[40], water toxicity and organoleptic potability screening[41,42]. The response of the E-tongue system to the two isoforms was analyzed by a pattern recognition method called Principal Component Analysis (PCA), to detect the similarities or differences in taste of the

sample solutions from time 0 (t0, just solubilized) to 30 minutes (t30) and after 60 minutes (t60). The PCA score plot representing the dispersion of E-tongue data obtained for the two isoforms shows completely different sensorial kinetics between KET-LYS P1 and KET-LYS P2. Firstly, the position on the gustatory map (determined by modelling sweet, bitter and salty solutions composition of the PCA score plot) is significantly different at t0 between the co-crystal and the salt forms, as KET-LYS P1 starts in the right lower quadrant of the map, while KET-LYS P2 is in the upper part of the left quadrant in an opposite position compared to KET-LYS P1 (Figure 6). These data demonstrate that the co-crystal at t0 is sweeter than the salt, and for this reason different coating processes or/and flavour addition can be envisioned for the potential subsequent development of the new salt KET-LYS P2 form compared to that usually followed during the manufacturing of the commercialized KLS (KET-LYS P1). Secondly, analysis at t30 and t60 show that KET-LYS P1 undergoes smaller variations in the first 60 minutes after preparation of the solution compared to KET-LYS P2, as over time, KET-LYS P1 remains in the same quadrant, while KET-LYS P2 makes a significant change in its position on the gustatory map in the first 30 min, moving from the upper part of the left quadrant to the lower right quadrant (Figure 6). This phenomenon could be due to the formation of intimate ion pairs in solution that maintain over time (from t0 to t60) the memory of the different stereochemistry of the original crystalline structures, and this results in a different solvation and shielding of the ion and the counterion of the KET-LYS P1 and KET-LYS P2 systems[43].

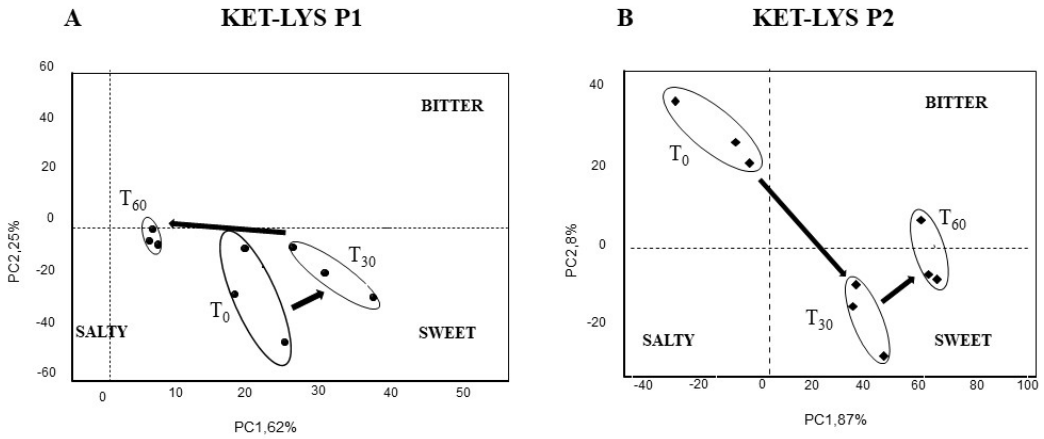

Figure 6. Taste and sensorial kinetic analysis by electronic tongue of co-crystal KET-LYS P1 and salt KET-LYS P2. PCA score plot of KET-LYS P1 and KET-LYS P2 over the time lapsed after dissolution preparation. T0, just solubilized; T30, 30 minutes in solution; T60, 60 minutes in solution. PC1: first principal component; PC2: second principal component. Three analytical replicates were performed for all the time points.

2.5. Pharmacokinetics in vivo of KET-LYS P1 and KET-LYS P2

Having assessed the differences in IDRs between the polymorphic salt and co-crystal forms of KET and LYS, we studied and compared the in vivo pharmacokinetics. We analysed the major pharmacokinetic parameters after oral administration of the two compounds at the dose of 3.5 mg/kg to not-fasted Sprague Dawley male rats. Results showed that the two polymorphs were comparable in terms of C_{max}, $T_{1/2}$, and mean residence time (MRT), but notably, dose-normalized area under the curve to infinity (AUC-inf) and T_{max} values of KET-LYS P1 were significantly higher than those of KET-LYS P2

(74076 ± 5931 ng/ml*h vs 50434 ± 4439 ng/ml*h, $p < 0.01$, for AUC-inf, and 3.1 ± 0.97 h vs 0.64 ± 0.34 h, $p < 0.05$ for T_{max}, for P1 and P2, respectively, n=6, mean ± SEM) (Figure 7). After single oral administration, AUC-inf measures the absorbed drug amount and is calculated from administration time to infinity (inf), and peak time (T_{max}) depends on the rate of drug absorption. Thus, the higher AUC-inf of the commercial KET-LYS P1 compared to that of the new isoform KET-LYS P2 means a higher amount of co-crystal KET-LYS P1 that has been absorbed, while KET-LYS P1 higher T_{max} indicates a slower absorption of this isoform compared to KET-LYS P2. This latter data agrees with IDR data showing the potential advantages of KET-LYS P2 for a further improvement of fast acting formulations.

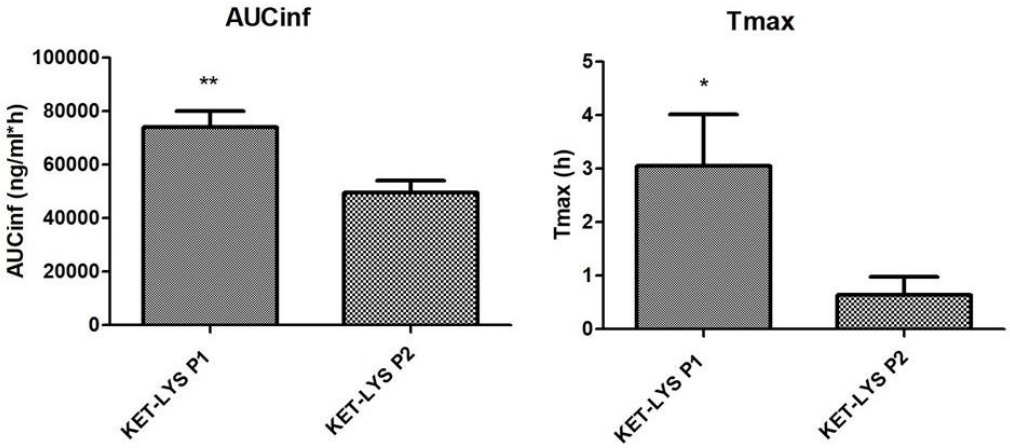

Figure 7. Pharmacokinetics *in vivo* of co-crystal KET-LYS P1 and salt KET-LYS P2. AUC-inf and T_{max} values of KET-LYS P1 and KET-LYS P2. * $p<0.05$ and ** $p<0.01$. Analyses were performed in n=6 rats and values are expressed as mean ± SEM.

While it can be expected that co-crystals and salts with different coformers have different physicochemical and pharmacokinetic characteristics, finding significant differences between the IDR, taste and pharmacokinetics of a salt and those of its co-crystal polymorph surely opens new perspectives. All together these differences clearly highlight the actual impact that (in this case) the substitution of one ionic bond (salt) with a neutral HB (co-crystal) can have on drug clinical performance, to the extent that different formulations and different coating processes or flavour addition can be suggested for the two isoforms. KLS is a widely used NSAID that is already known – and our data on KET-LYS P1 Tmax confirm it ¬– for its rapid absorption and subsequent therapeutic action[22], which make it indicated for the treatment of acute inflammatory and painful conditions. From our data, we can hypothesize that new polymorphic form KET-LYS P2 could further emphasize the property of KLS for the treatment of acute inflammatory and painful conditions.

4. Materials and Methods

4.1 Crystallization conditions screen to identify potential polymorphs

To deeply investigate the solid-state characteristics of KLS, we conducted a polymorph screening study to identify all the crystalline forms that this API can adopt. To this end, several crystallization conditions were tested based on the solubility properties of the

compounds. Experiments were performed by: *i)* dry grinding, in which solid forms of both coformers were combined for manual/mechanical grinding for a fixed period; *ii)* kneading (liquid assisted grinding), in which solid forms of both coformers were combined in the presence of a very small amount of solvent for manual/mechanical grinding for a fixed period; *iii)* slurry, in which solid forms of both coformers were added to a solvent/solvent mixture for a fixed period of equilibration with the solid remaining in excess for the duration of the experiment; *iv)* evaporation at low/room/high temperature (based on boiling point), in which the solvent was removed from an undersaturated solution of both coformers via evaporation at various temperatures; *v)* precipitation by antisolvent addition, in which co-crystallization directly resulted after the addition of an antisolvent to a solution of both coformers.

For all the compounds, various stoichiometric ratios were investigated in the range of 0.5 to 2 equivalents with respect to the amount of KET or (L)-LYS. The slurry experiment with saturated solutions in various solvents was performed when possible.

4.2 General Procedure for the preparation of KET-LYS Polymorph 1 (P1)

50 g of (RS)-KET were added to 350 mL of ethanol, the mixture was stirred at RT until complete solubilization. 29 g of (DL)-LYS, 50% w/w in water (1:1 ratio) were added and the solution was stirred at RT until the first precipitation occurred. The mixture was left under these conditions for 3 h and then cooled to 5 °C. After 5 h the product was recovered by filtration, washed with 60 mL of ethanol and dried under reduced pressure at 40 °C. The final KET-LYS P1 was obtained as white powder (69 g, yield of 88%).

4.3 General Procedure for the preparation of KET-LYS Polymorph 2 (P2)

1.2 g of (RS)-KET and 0.69 g of (DL)-LYS (1:1 ratio) were suspended in 20 mL of methanol and left under stirring at 40 °C for 1 h. The suspension was then filtered (0.45 μm filter) directly in a Mettler Toledo Easymax 102 reactor. The solution was left under stirring for 5 minutes in the reactor, then 100 mL of ethyl acetate was added, and the solution was cooled down to -5 °C without solid formation. Additional ethyl acetate (20 mL) was added through pipette in two aliquots (10 mL and 10 mL) to trigger nucleation. The system was left under stirring until the suspension became "milky". Additional 30 minutes of stirring was applied. The precipitate was then filtered, and the collected sample was stored in a sealed vial at room temperature. The final KET-LYS P2 was obtained as white powder (1.3 g, yield of 69%).

4.4 X-ray Powder Diffractometry (XRPD)

XRPD experiments were performed on a powder X-ray diffractometer (Rigaku MiniFlex600) using Cu Kα radiation (1.540598 Å). Samples were scanned with a step size of 0.01° (2θ) and speed 10.0°/min (2θ) from 3° to 40° 2θ. The tube voltage and amperage were 40 kV and 15 mA, respectively.

4.5 Thermal Analyses

The analyses were carried out using the Mettler Toledo TGA/DSC1. Samples were weighed in an aluminum pan hermetically sealed with an aluminum pierced cover. The analyses were performed heating the sample from 25 °C to 320 °C at 10 °C/min.

4.6 Fourier-transform infrared spectroscopy (FT-IR)

The analysis was carried out using a Thermo Nicolet iS50 - ATR module Spectrometer equipped with: Smart Performer Diamond, DTGS KBr Detector, IR Source, KBr Beam splitter.

4.7 Solid-state NMR characterization

Solid-state NMR (SSNMR) spectra of KET, LYS, $Na^{+}KET^{-}$, and KET-LYS P1 were acquired with a Bruker Avance II 400 Ultra Shield instrument, operating at 400.23, 100.63 and 40.56 MHz, respectively for ^{1}H, ^{13}C and ^{15}N nuclei.

Powder samples were packed into cylindrical zirconia rotors with a 4 mm o.d. and an 80 μL volume. A certain amount of sample was collected from each batch and used without further preparations to fill the rotor. 13C CPMAS spectra were acquired at a spinning speed of 12 kHz, using a ramp cross-polarization pulse sequence with a 90° 1H pulse of 3.60 μs, a contact time of 3 ms, optimized recycle delays between 1.5 and 3.5 s, a number of scans in the range 430-640, depending on the sample. 15N CPMAS spectra were acquired at a spinning speed of 9 kHz using a ramp cross-polarization pulse sequence with a 90° ^{1}H pulse of 3.60 μs, a contact time between 1 and 4 ms, optimized recycle delays between 1.1 and 3.4 s, a number of scans in the range 14330-22770, depending on the sample. For every spectrum, a two-pulse phase modulation (TPPM) decoupling scheme was used, with a radiofrequency field of 69.4 kHz. The ^{13}C chemical shift scale was calibrated through the methylenic signal of external standard glycine (at 43.7 ppm). The ^{15}N chemical shift scale was calibrated through the signal of external standard glycine (at 33.4 ppm with reference to NH3).

2D ^{1}H–^{13}C on- and off-resonance (short and long-range, respectively) HETCOR spectra were measured with contact times of 0.1 and 7 ms, respectively, and FSLG t1 decoupling and TPPM t2 decoupling (rf fields of 82 kHz). 288 and 384 scans were averaged for 88 and 128 increments, respectively with 3.4 s of relaxation delay. The indirect 1H chemical shift scale in the HETCOR spectra was experimentally corrected by a scaling factor of $1/\sqrt{3}$ because the 1H chemical-shift dispersion is scaled by a factor of $1/\sqrt{3}$ during FSLG decoupling.

The ^{13}C CPMAS spectrum of KET-LYS P2 was acquired with a Jeol ECZR 600 instrument, operating at 600.17 and 150.91 MHz, respectively for ^{1}H and ^{13}C nuclei. The powder sample was packed into a cylindrical zirconia rotor with a 3.2 mm o.d. and a 60 μL volume. A certain amount of sample was collected from the batch and used without further preparations to fill the rotor. The ^{13}C CPMAS spectrum was acquired at 273 K, at a spinning speed of 20 kHz, using a ramp cross-polarization pulse sequence with a 90° 1H pulse of 2.19 μs, a contact time of 3.5 ms. An optimized recycle delay of 6 s was used, for number of scans of 240. A two-pulse phase modulation (TPPM) decoupling scheme was used, with a radiofrequency field of 108.5 kHz. The ^{13}C chemical shift scale was calibrated through the methylenic signal of external standard glycine (at 43.7 ppm).

Several attempts were made for acquiring the ^{15}N CPMAS spectrum of KET-LYS P2 by changing several parameters (contact time, number of scans, Hartmann-Hahn conditions, …) without succeeding.

4.8 Intrinsic dissolution rate

KET-LYS P1 and KET-LYS P2 were tested for intrinsic dissolution rate (IDR). IDR experimental method was performed using 150 mg powder sample; this was compacted by means of a hydraulic press in a round Ø = 11 mm matrix, under approximately 2 tons force for 3 min. The obtained compacts were maintained inside the matrix and tested in

a USP42 Apparatus 2 (Distek Dissolution System 2100B) under the following conditions: 500 mL of gastric simulated fluid (GSF) without pepsin, 37 °C and 30 rpm paddle rotation speed. The amount of solid dissolved at each time point was determined spectrophotometrically at 260 nm. The test was performed in 3 replicates. Statistical analysis of the data was performed by Microsoft Excel.

4.9 Multisensory analysis

The composition and properties of tested samples (KET-LYS P1 and KET-LYS P2) are listed in Table S1. The response of E-tongue system was tested in model solutions of salty, bitter and sweet taste for which aqueous solutions of 0.001 mol/L NaCl, 0.001 mol/L $MgCl_2$ and 0.06 mol/L of fructose were used respectively. Millipore grade water was used for aqueous solution preparation. All the other chemicals were of analytical grade and used without further purification.

Membrane components, high molecular weight poly(vinyl chloride) (PVC), bis(2-ethylhexyl) sebacate (DEHS) plasticizer, tridodecylmethyl ammonium chloride (TDMACl), potassium tetrakis-(4-chlorophenyl)borate (TpClPBK) lipophilic additives, and nonactine ionophore were purchased from Sigma-Aldrich (Rome, Italy). Tetrahydrofuran (THF) used for PVC membranes preparation was obtained from Carlo Erba Reagents (Rome, Italy) and distilled prior to use. 5,10,15,20-Tetraphenylporphyrin manganese(III) chloride ionophore [Mn(TPP)Cl] was synthesized in our laboratories and fully characterized according to the literature procedure[23]. Millipore grade water was used for aqueous solution preparation. All the other chemicals were of analytical grade and used without further purification.

The potentiometric E-tongue system was composed of 8 sensors with three different types of sensing membranes: PVC-based solvent polymeric membranes doped with Mn(TPP)Cl (sensor A1) and nonactin (sensor C1) ionophores; and chalcogenide glass membranes doped with different metal salts (G2-Cu, G7-Tl, G8-Ag, G10-Cd, G11-Pb) and sensor A7 with polycrystalline LaF_3 membrane. The PVC-based solvent polymeric membranes were prepared according to the previously reported procedures[24,25]. For this, all the membrane components (PVC 30–33 wt%, plasticizer 60–66 wt%, ion-exchanger 0.1–10 wt%, and 1 wt% of ionophore) were dissolved in THF. The membrane cocktails were then cast in a 24 mm i.d. glass ring on a glass slide and the solvent was evaporated overnight. The polymeric membrane discs of 8 mm in diameter were cut out from the parent membrane and fixed with 10 wt% of PVC in cyclohexanone glue onto hollow PVC tubes that served as electrode bodies, filled with 0.01 mol/L solutions of NaCl and NH4C1 for sensor A1 and sensor C1 respectively. The sensor A1 and C1 membrane potential was registered against the internal, homemade Ag/AgCl reference electrode.

Chalcogenide glass sensors and sensor A7 with a polycrystalline LaF_3 membrane had solid Cu-wire/Ag-paste solid contacts and were purchased from Sensor Systems (St. Petersburg, Russia). The potentials of E-tongue system sensors were measured versus a saturated calomel reference electrode (SCE, AMEL, Milan, Italy), in a standard two-electrode configuration cell. Potentiometric measurements were performed with LiquiLab (ECOSENS srl, Rome, Italy) high-impedance analog-to-digital potentiometer. Prior to measurements, the sensors were soaked in 0.01 mol/L NaCl aqueous solution for at least 24 h.

The quantity of samples KET-LYS P1 and KET-LYS P2 corresponded to the standard dosage of administration of commercial KLS: 40 mg. This amount of sample was dissolved in 20 mL of distilled water.

All analyses were performed in analytical triplicate for all the above time conditions. The pH value and electrical conductivity of the t24h and t48h solutions were also measured. The samples were stored in closed containers at room temperature (+22 °C) during the study period.

4.10 Pharmacokinetics

For the pharmacokinetics studies, Sprague Dawley male rats (body weights 250-275 g at the time of the treatment) were used. The animals were originally supplied by Harlan, Italy. The animals were acclimatized to local housing conditions for approximately 5 days.

The animals were housed in a single, exclusive room, air conditioned to provide a minimum of 15 air changes/hour. The environmental controls were set to maintain temperature within 22°C and relative humidity within the range 50 to 60% with an approximate 12 hour light and 12 hour dark cycle that is controlled automatically. Food (Mucedola Standard GLP diet) and water were available ad libitum throughout the study. All animals were weighed on the day of each treatment. Clinical signs were monitored at regular intervals throughout the study in order to assess any reaction to treatment. Each animal was uniquely identified with a colored spray on the back before the experiment.

The compounds were administered at a dose of 3.5 mg/kg as KET free acid in gelatine capsules (size 9, Torpac®). To perform this, capsules were individually filled and weighed up with the substances and then filled with rice starch up to about 20 mg weighed again and closed. After administration, blood (approximately 60-80 µL) was sampled from tail vein at the following timepoints: 15 min, 30 min, 1, 2, 4, 6, 8, and 24h and 48h. Blood samples were collected in heparinized eppendorfs (Heparin Vister 5000U.I/mL), gently mixed and placed immediately on ice; then eppendorfs were centrifuged (3500xg, at 4°C for 15 min) and the resulted plasma collected and transferred to uniquely labelled eppendorfs and frozen at –20°C till the HPLC-MS analysis.

At the end of the study animals were sacrificed by exanguination under deep isoflurane anesthesia.

The experiment was carried on in agreement with the Italian Law D. L.vo 4 marzo 2014, n. 26.

4.11 Statistics

For IDR experiments, the statistical analysis of the data was performed by Microsoft Excel. For pharmacokinetics experiments, data were expressed as mean ± standard error of the mean (SEM). Multiple statistical comparisons between groups were performed by two-tailed unpaired Student's t-test. All data collected follow with good approximation a normal distribution, being included in the 95% confidence interval of the mean; this generally allows for the clear identification of outliers, if any, and for the application of the statistical analyses described above. No outliers were found during the present study. Missing data in the results were then related only to overt technical issues during the experimental procedures, which led to the exclusion of those specific samples from the analysis.

5. Conclusions

In this study, we synthesized and characterized, for the first time, two different polymorphic forms of KLS, a co-crystal, KET-LYS P1, and a salt, KET-LYS P2. Through advanced and sophisticated analyses, we were able to undoubtedly define the structural characteristics of the two isoforms and to compare their physicochemical characteristics, in terms of dissolution rate and taste, and pharmacokinetic profiles *in vivo*. What emerged is that, from a structural point of view, the commercial KLS should be more appropriately defined as a co-crystal (KET-LYS P1) rather than a salt, and that the newly identified salt KET-LYS P2 has significantly different chemical and pharmacokinetic characteristics compared to KET-LYS P1. The faster dissolution rate and reduced T_{max} in vivo of KET-LYS P2 suggest potential advantages of this new form for fast acting formulations of the drug. Nevertheless, it should be considered that this new isoform may exhibit a more bitter taste and a lower AUC compared to the commercially available KLS form, and this should prompt the design of specific formulation studies to hypothesize different potential formulations (faster release) and coating or flavouring processes, based on the specific characteristics of the starting API material.

The present study advances our knowledge regarding the solid-state characteristics of KLS and gives a comprehensive view of its polymorphic diversity; while doing this, it led to the discovery of a new polymorph of KLS, KET-LYS P2, thus opening the way for the development of a new potential KET-LYS polymorph drug, the pharmacological and pharmacokinetic characteristics of which will be further investigated to define the appropriate formulation and the conditions that would most benefit from the treatment with this drug.

6. Patents

Composition, process of production and uses of co-crystal polymorph of KLS (KET-LYS P1) is described in Patent number WO2020126088A1.

Supplementary Materials: The following are available online at www.mdpi.com/xxx/s1. Table S1: Tested samples and model taste solutions for E-tongue analysis. Figure S1: DSC profile of KET-LYS P1, Figure S2: DSC profile of KET-LYS P2, Figure S3: FT-IR spectrum of KET-LYS P1, Figure S4: FT-IR spectrum of KET-LYS P2, Figure S5: Crystal structure of (L)-lysine, Figure S6: ^{13}C CPMAS spectra of samples KET, (L)-LYS, Na+KET-, (DL)-LYS·2HCl, KET-LYS P1 and KET-LYS P2, Figure S7: Crystal structure of (RS)-KET displaying the typical carboxylic homodimeric synthon, Figure S8: On-resonance ^{1}H-^{13}C FSLG HETCOR spectrum (contact time = 0.1 ms) of KET-LYS P1, Figure S9: XRPD pattern comparison between KET-LYS P1 and commercial KLS.

Author Contributions: Conceptualization, A.A.; methodology, A.A., B.G., S.L., S.B., M.T.,S.M.,L.L.,R.P. and M.R.C.; validation, B.G., S.L., S.B., M.T., S.M., L.L., R.P. and M.R.C.; formal analysis, B.G., S.L., S.B., M.T., S.M., L.L. and R.P; data curation, R.N.; writing—original draft preparation, A.A., B.G, S.B. and M.R.C; writing—review and editing, R.N.; supervision, A.A. and M.A; funding acquisition, S.L. All authors have read and agreed to the published version of the manuscript.

Funding: This research was funded by the Italian Ministry of Education, University and Research, Research Project AMICO (code ARS01_00758).

Institutional Review Board Statement: The study was conducted according to the guidelines of the the Italian Law D. L.vo 4 marzo 2014, n. 26, and approved by the Italian Ministry of Health (433/2016-PR of April 27th 2016).

Acknowledgments: The Authors are grateful to Aphad S.r.l. (Milan, Italy) for having performed the pharmacokinetic studies.

Conflicts of Interest: Andrea Aramini, Gianluca Bianchini, Samuele Lillini, Mara Tomassetti, Rubina Novelli, Simone Mattioli and Marcello Allegretti are employees of Dompé Farmaceutici s.p.a., Italy. The company has interest in the development of compounds for the treatment of inflammatory and painful conditions. The other authors declare no conflict of interest.

References

1. N. K. Duggirala, M. L. Perry, Ö. Almarsson, M. J. Zaworotko, Chem. Commun. 2015, 52, 640–655.
2. M. Karimi-Jafari, L. Padrela, G. M. Walker, D. M. Croker, Cryst. Growth Des. 2018, 18, 6370–6387.
3. X.-L. Dai, J.-M. Chen, T.-B. Lu, CrystEngComm 2018, 20, 5292–5316.
4. C. B. Aakeröy, M. E. Fasulo, J. Desper, Mol. Pharm. 2007, 4, 317–322.
5. R. Chadha, S. Bhandari, J. Haneef, S. Khullar, S. Mandal, CrystEngComm 2014, 16, 8375–8389.
6. Ö. Almarsson, M. J. Zaworotko, Chem. Commun. 2004, 1889–1896.
7. S. Tothadi, T. R. Shaikh, S. Gupta, R. Dandela, C. P. Vinod, A. K. Nangia, Cryst. Growth Des. 2021, 21, 735–747.
8. D. Bernasconi, S. Bordignon, F. Rossi, E. Priola, C. Nervi, R. Gobetto, D. Voinovich, D. Hasa, N. T. Duong, Y. Nishiyama, M. R. Chierotti, Cryst. Growth Des. 2020, 20, 906–915.
9. B. R. Bhogala, S. Basavoju, A. Nangia, CrystEngComm 2005, 7, 551–562.
10. A. J. Cruz-Cabeza, CrystEngComm 2012, 14, 6362–6365.
11. S. L. Childs, G. P. Stahly, A. Park, Mol. Pharm. 2007, 4, 323–338.
12. P. Stainton, T. Grecu, J. McCabe, T. Munshi, E. Nauha, I. J. Scowen, N. Blagden, Cryst. Growth Des. 2018, 18, 4150–4159.
13. E. Losev, E. Boldyreva, Acta Crystallogr. Sect. C Struct. Chem. 2018, 74, 177–185.
14. E. A. Losev, E. V. Boldyreva, CrystEngComm 2018, 20, 2299–2305.
15. S. R. Perumalla, C. Wang, Y. Guo, L. Shi, C. C. Sun, CrystEngComm 2019, 21, 2089–2096.
16. C. L. Jones, J. M. Skelton, S. C. Parker, P. R. Raithby, A. Walsh, C. C. Wilson, L. H. Thomas, CrystEngComm 2019, 21, 1626–1634.
17. A. V. Trask, Mol. Pharm. 2007, 4, 301–309.
18. K. Raza, P. Kumar, S. Ratan, R. Malik, S. Arora, SOJ Pharm. Pharm. Sci. 2014, 1.
19. K.-S. Seo, R. Bajracharya, S. H. Lee, H.-K. Han, Pharmaceutics 2020, 12, DOI 10.3390/pharmaceutics12090853.
20. L. Miles, J. Hall, B. Jenner, R. Addis, S. Hutchings, Curr. Med. Res. Opin. 2018, 34, 1483–1490.
21. R. Altman, B. Bosch, K. Brune, P. Patrignani, C. Young, Drugs 2015, 75, 859–877.
22. G. Varrassi, E. Alon, M. Bagnasco, L. Lanata, V. Mayoral-Rojals, A. Paladini, J. V. Pergolizzi, S. Perrot, C. Scarpignato, T. Tölle, Adv. Ther. 2019, 36, 2618–2637.
23. J. E. Falk, K. M. Smith, Eds. , Porphyrins and Metalloporphyrins: A New Edition Based on the Original Volume by J. E. Falk, Elsevier Scientific Pub. Co, Amsterdam ; New York, 1975.
24. S. S. Levitchev, A. L. Smirnova, V. L. Khitrova, L. B. Lvova, A. V. Bratov, Yu. G. Vlasov, Sens. Actuators B Chem. 1997, 44, 397–401.
25. L. Lvova, C. Natale, A. D'Amico, R. Paolesse, J. Porphyr. Phthalocyanines 2009, 13, 1168–1178.
26. R. M. Silverstein, F. X. Webster, D. J. Kiemle, D. L. Bryce, Spectrometric Identification of Organic Compounds, Wiley, Hoboken, NJ, 2015.
27. P. Cerreia Vioglio, M. R. Chierotti, R. Gobetto, Adv. Drug Deliv. Rev. 2017, 117, 86–110.
28. M. R. Chierotti, R. Gobetto, Chem. Commun. 2008, 1621–1634.
29. P. Briard, J. C. Rossi, Acta Crystallogr. Sect. C 1990, 46, 1036–1038.
30. S. Chen, H. Xi, R. F. Henry, I. Marsden, G. G. Z. Zhang, CrystEngComm 2010, 12, 1485–1493.
31. W. Pa, H. Ce, H. Kd, Angew. Chem. Int. Ed Engl. 2015, 54, 3973–3977.
32. P. Pudjiastuti, S. Wafiroh, E. Hendradi, H. Darmokoesoemo, M. Harsini, M. A. R. D. Fauzi, L. Nahar, S. D. Sarker, Open Chem. 2020, 18, 226–231.
33. C. R, J. Stem Cell Biol. Transplant. 2017, 1, DOI 10.21767/2575-7725.100012.
34. H. Sohi, Y. Sultana, R. K. Khar, Drug Dev. Ind. Pharm. 2004, 30, 429–448.
35. A. R. B., S. Shaarani, Int. Food Res. J. 2015, 22, 731–738.
36. M. Maniruzzaman, J. S. Boateng, B. Z. Chowdhry, M. J. Snowden, D. Douroumis, Drug Dev. Ind. Pharm. 2014, 40, 145–156.
37. M. F. Arafa, S. A. El-Gizawy, M. A. Osman, G. M. El Maghraby, Drug Dev. Ind. Pharm. 2016, 42, 1225–1233.
38. Y. Maeno, T. Fukami, M. Kawahata, K. Yamaguchi, T. Tagami, T. Ozeki, T. Suzuki, K. Tomono, Int. J. Pharm. 2014, 473, 179–186.
39. S. Aitipamula, A. B. H. Wong, P. Kanaujia, J. Pharm. Sci. 2018, 107, 604–611.
40. L. L, D. S, B. A, M. P, S. C, V. C, D. N. C, P. R, T.-B. P, F. G, Talanta 2012, 97, 171–180.
41. L. Lvova, C. Guanais Gonçalves, K. Petropoulos, L. Micheli, G. Volpe, D. Kirsanov, A. Legin, E. Viaggiu, R. Congestri, L. Guzzella, F. Pozzoni, G. Palleschi, C. Di Natale, R. Paolesse, Biosens. Bioelectron. 2016, 80, 154–160.

42. L. Lvova, I. Jahatspanian, L. H. C. Mattoso, D. S. Correa, E. Oleneva, A. Legin, C. Di Natale, R. Paolesse, Sensors 2020, 20, DOI 10.3390/s20030821.
43. J. Hack, D. C. Grills, J. R. Miller, T. Mani, J. Phys. Chem. B 2016, 120, 1149–1157.